Suppression of Spin-Orbit Scattering in Strong-Disordered Gold Nanojunctions

A. Anaya, M. Bowman, and D. Davidović
Georgia Institute of Technology, Atlanta, GA 30332
(Dated: February 2, 2008)

We discovered that spin-orbit scattering in strong-disordered gold nanojunctions is strongly suppressed relative to that in weak-disordered gold thin films. This property is unusual because in weak-disordered films, spin-orbit scattering increases with disorder. Granularity and freezing of spin-orbit scattering inside the grains explains the suppression of spin-orbit scattering. We propose a generalized Elliot-Yafet relation that applies to strong-disordered granular regime.

The field of spintronics has recently emerged as a potential alternative to conventional charge-based electronics. [1] What sets spintronics apart is the explicit study or use of the electron spin degree of freedom. A challenge in spintronics is the finite lifetime of spin-polarized current, since electron spins can flip in normal metals and semiconductors.

It is generally accepted that a spin-orbit (SO) interaction, through the so called Elliot-Yafet mechanism, [2, 3] causes spin-flip scattering in weak-disordered metals. In this mechanism, the SO scattering time (τ_{so}^{ey}) is proportional to the momentum relaxation time τ, $\tau_{so}^{ey} = \tau/\alpha$, which is known as the Elliot-Yafet relation. The scattering ratio $\alpha \ll 1$ represents the spin-flip probability during the momentum relaxation time. It depends on the atomic number, band structure, and to a lesser extent, on sample preparation techniques. It has recently been demonstrated that the Elliot-Yafet relation agrees with measured SO scattering time in a wide range of weak-disordered metallic samples. [4]

In this paper we investigate SO scattering in strong-disordered metals, that is, in metals where conduction electrons undergo transition into Anderson localized states at low temperatures. We find that the relation between disorder and SO scattering time in the strong-disordered regime is qualitatively different from that in the weak-disordered regime. We observe a strong enhancement of the SO scattering time compared to that in weak-disordered samples. We propose that the enhancement of the SO scattering time arises from granularity, as follows.

Consider a 3D granular system composed of grains with average diameter D and average grain-to grain resistance R_g. If R_g is larger than $R_Q = h/e^2 = 25.8k\Omega$, within a factor of order one, then the system is strong-disordered. If $R_g < R_Q$, within a factor of order one, then the system is weak-disordered. [5]

By definition, R_g is larger than the resistance inside the grains. The dwell time of an electron on any given grain (t_D) is roughly $t_D = t_H R_g/R_Q$, where $t_H = h/\delta$ is the Heisenberg time (δ is the level spacing).

We consider small strong-disordered granular samples, in which the electron localization length is larger than sample size. In these samples, electrons at the Fermi level are spatially extended through the sample.

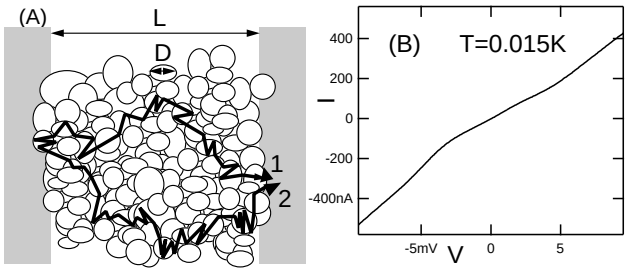

FIG. 1: A. Sketch of a granular sample and two semi-classical electron trajectories traversing the sample. B. I-V curve of a sample smaller than the localization length.

We discuss SO scattering time of electrons at the Fermi level and at zero temperature. We assume the grains are ballistic so that momentum relaxation is dominated by surface scattering. So the Elliot-Yafet relation predicts a SO scattering time of $\tau_{so}^{ey} = D/(\alpha v_F)$. We argue that τ_{so}^{ey} is not a good estimate of the spin-orbit scattering time if the grains are sufficiently small and R_g is large enough.

If the grains were completely isolated, the strength of SO interaction would be governed by a dimensionless parameter t_H/τ_{so}^{ey}, and SO scattering inside the grains would be weak if $t_H < \tau_{so}^{ey}$. [6, 7] In this case, the electronic wavefunctions of the grain are nearly all spin-up or all spin-down.

Reducing the grain diameter decreases both t_H and τ_{so}^{ey}, as $t_H \sim \frac{D^3}{v_F \lambda_F^2}$ and $\tau_{so}^{ey} \sim \frac{D}{\alpha v_F}$, respectively. Since t_H decreases faster than τ_{so}^{ey}, a borderline diameter $D^\star$ exists, below which SO scattering is weak. From $t_H \sim \tau_{so}^{ey}$, we obtain $D^\star = \lambda_F/\sqrt{\alpha}$.

In a granular system as in Fig. 1-A, once an electron is localized within any given grain, its motion is governed by the wavefunctions of the grain. If $D < D^\star$, the spin-flip probability inside the grain would be small, even if $t_D > \tau_{so}^{ey}$, because SO scattering in individual grains freezes after the Heisenberg time. [6, 7]

Since SO scattering inside the grains with $D < D^\star$ is weak, we propose that electrons at the Fermi level at zero temperature may flip spin only when they hop between neighboring grains, with a spin-flip probability α. This leads to an estimate

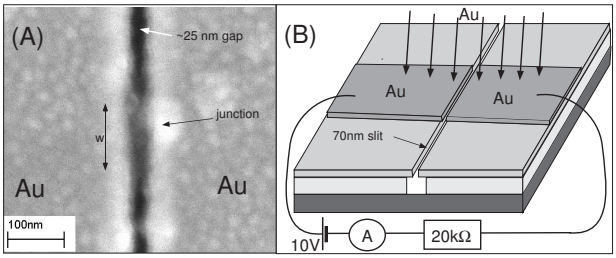

FIG. 2: A. Image of a strong-disordered Au nano-junction. B. Fabrication of strong-disordered Au nanojunctions.

$$\tau_{so} = \frac{t_D}{\alpha} \sim \frac{D^3}{\alpha v_F \lambda_F^2} \frac{R_g}{R_Q}. \quad (1)$$

This equation generalizes the Elliot-Yafet relation for granular systems. An interesting feature of this equation is that the SO scattering time is proportional to the resistance between grains. The resistivity is $\rho \sim R_g D$, hence an increase in resistivity leads to an increase in SO scattering time, a behavior opposite to that found in weak-disordered homogeneous metals, since τ_{so} is enhanced at the expense of dwell time.

We use electron transport in strong-disordered gold nanojunctions to investigate SO scattering in the strong-disordered regime. An image of one nanojunction, from a scanning electron microscope, is shown in Fig. 2-A. We create these nanojunctions by making electric contacts between two Au films at large bias voltage. [8, 9]

To summarize, Au atoms are deposited in high vacuum over two bulk Au films separated by a $\sim$ 70nm slit, as sketched in Fig. 2-B. The applied voltage is 10 Volt and the current is measured during the deposition, to detect the moment of contact, at which point the evaporation is stopped and the voltage is reduced. Large voltage introduces strong-disorder in the nanojunction, through processes such as electromigration, surface atom diffusion, and intermixing with H_2O and O_2 molecules. [8]

Au films to the left and right of the nanojunction are good metals with resistivity $\approx 35\mu\Omega cm$. Through scanning electron microscopy combined with in situ transport measurements, we determined that the nanojunctions were homogeneous at length scale comparable to the gap size (we determined that the sample resistance was inversely proportional to width w in Fig. 1). The resistivity of the material inside the nanojunction was estimated to be $\rho \approx 1 \cdot 10^5 \mu\Omega cm$. [9] This value is larger than the so called "maximum metallic resistivity" of $200\mu\Omega cm$. Thus, the nominal transport mean free path (l), obtained from $\rho = m v_F / n e^2 l$, is $l \approx 0.01\mathring{A}$, much shorter than the Fermi wavelength.

The short mean free path indicates that Au in the nanojunction is very disordered. We have explained the disorder by granularity and the grain size much smaller than the nanojunction dimensions. [9] In particular, the disorder could not be amorphous as Au did not alloy with the impurities that were present in sample fabrication (H_2O or O_2). Our imaging resolution, however, was insufficient to determine the grain diameter. Recently, it has been demonstrated that large bias voltages applied to Au surfaces can induce electrochemical processes that lead to formation of Au nanoparticles of diameter on the order of a few nanometer, [10, 11] and these nanoparticles self-assemble into a granular structure. [11]

In the prior work, [9] we showed that the electron localization length in the nanojunction is finite at low temperatures. To summarize, samples with resistance larger than approximately R_Q displayed Coulomb blockade. The width of these samples was smaller than approximately 50 nm. The Coulomb blockade was attributed to electron tunnelling on and off the localized electronic wavefunctions inside the junction. From the temperature dependence of the conductance in the Coulomb blockade, we determined that the localization length exceeded 20nm.

In addition, samples with resistance smaller than about $0.5R_Q$ did not exhibit Coulomb Blockade at $T = 0.015K$. The I-V curve of these samples at $T = 0.015K$ was linear around zero bias voltage. The dependence of the Coulomb blockade on sample resistance was analogous to that found in strong-disordered InO_X mesoscopic semiconductors. [12]

The absence of Coulomb blockade in low resistance samples was explained by the localization length exceeding the nanojunction length. In this regime, the electronic wavefunctions extended from one reservoir to another reservoir and quantum electron transport could be described using models based on weak-disorder theories. For this letter, we select these low resistance samples, because quantum interference effects are easier to interpret in these samples.

Note that in a granular system, the transport mean free path can be much shorter than the Fermi-wavelength even in the metallic state at zero temperature. [13] Thus, it is not unphysical that the electron wavefunctions extend through the nanojunction, despite the fact that the transport mean free path is $\ll \lambda_F$.

The standard technique to measure τ_{SO} in disordered conductors is weak-localization, [14] the effect that originates from the orbital effect of the applied magnetic field on the electron wavefunctions. In our samples, however, the nominal transport mean free path is shorter than λ_F, and we show that in this case the Zeeman effect is stronger than the orbital effect. We introduce a new technique to measure a τ_{so} lower bound.

We determined that τ_{so} lower bound varies weakly among low resistance samples, down to the samples with resistance below $0.1R_Q$. The I-V curve of sample 2 (Fig. 1-B) is linear at zero bias voltage. It has only a weak suppression of differential conductance near zero

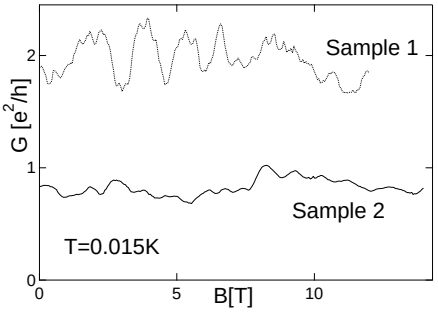

FIG. 3: A: Differential conductance versus magnetic field.

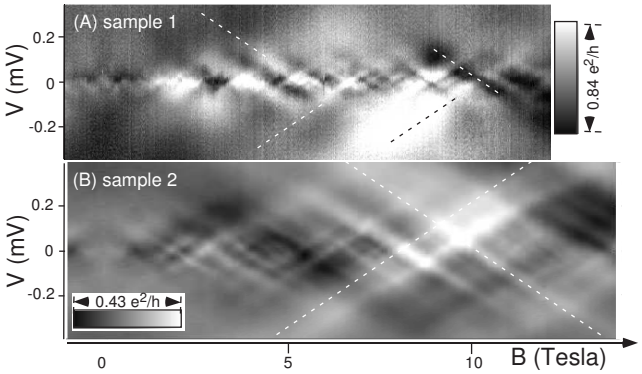

FIG. 4: Differential conductance versus magnetic field and bias voltage in samples 1 and 2 at $T = 0.015K$.

bias voltage, which is a Coulomb-Blockade precursor. [8]

A lock-in technique, with a $2\mu V$ excitation voltage, measures the differential conductance (G). Fig. 3-A shows G versus B in samples 1 and 2. The conductance clearly exhibits fluctuations with the magnetic field. The fluctuations are consistent with universal conductance fluctuations or what are known as magnetofingerprints, because: 1) the amplitude of the fluctuations is $\sim e^2/h$; 2) fluctuations are reproducible with field sweep; and 3) fluctuations are uncorrelated when samples are thermally cycled.

Magnetofingerprints in our samples differ from those in weak-disordered metals, in that they are caused by the Zeeman effect, not by the Aharonov-Bohm effect. The gray-scale image in Fig. 4 displays differential conductance versus bias voltage and magnetic field ($G(V, B)$). The main signature of the data is a structure in conductance which shifts linearly with V and B, with pronounced lines in $V - B$ parameter space. Some of the lines are highlighted with dashed lines of the form $eV \pm 2\mu_B B = const$. By comparison, in weak disordered metallic samples where the mean free path is longer than Fermi wavelength, the fluctuations with field and the fluctuations with voltage are uncorrelated. [14]

Consider quantum interference among two semiclassical electron pathways through the sample, depicted in Fig. 1-A. The interference depends on the phase difference ϕ between the probability amplitudes of the trajectories, and can be constructive or destructive, depending on whether $\phi = 2n\pi$ or $\phi = (2n + 1)\pi$, where $n = 0, \pm 1, ...$ For reference, we recall that the characteristic magnetic field for the Aharonov-Bohm effect is given by the field for a flux quantum $\Phi_0 = h/2e$ over the sample area, $B_{AB} = \Phi_0/L^2$. [14]

In a magnetic field, Zeeman splitting causes spin-up and spin-down electrons to have different Fermi wavelengths, hence spin-dependent contribution to ϕ. We find the contribution is $\sigma\mu_B B(t_2 - t_1)/\hbar$, where $\sigma = \pm 1$ corresponds to the spin direction and $t_{1,2}$ are the times of flight along the trajectories. Typical times of flight are $L^2/v_F l$, where l is the transport mean free-path. The Zeeman effect becomes significant when $\phi \sim 1$, and the characteristic field for the Zeeman effect is $B_Z = \frac{l}{\lambda_F}\frac{\Phi_0}{L^2}$. Thus, conductance fluctuations are spin-based if $B_Z/B_{AB} = l/\lambda_F < 1$. Our sample parameters are such that $B_Z/B_{AB} = l/\lambda_F < 1$.

If the bias voltage is nonzero, then electrons injected from the Fermi level have a voltage dependent contribution to ϕ, which is $\int_0^{t_1} eV(t)dt/\hbar - \int_0^{t_2} eV(t)dt/\hbar$. In Ohmic samples, the voltage drop is linear in space, and the contribution becomes $eV(t_1 - t_2)/(2\hbar)$. Thus,

$$\phi = eV(t_1 - t_2)/(2\hbar) + \sigma\mu_B B(t_1 - t_2)/\hbar.$$

For any given pair of trajectories, the voltage dependent contribution is proportional to the spin-dependent contribution. It follows that if both V and B are varied with a constraint that $eV + \sigma 2\mu_B B = const$, then the interference of an electron with spin σ is unchanged. As a result, the conductance of electrons with spin σ is constant when $eV + \sigma 2\mu_B B = const$, explaining Fig. 4.

We have neglected SO scattering in the analysis. In the following paragraphs, we take SO scattering into account. SO scattering does not destroy phase coherence [15] and we need to obtain ϕ in the presence of SO scattering.

Assume SO scattering to be strong, $\tau_{so} \ll t$, where t is the typical time of flight defined above. In this case, phase coherence survives only in the singlet channel, in which an electron traversing one trajectory with spin-up interferes with itself after traversing a second trajectory with spin-down. [15] The phase-shift in the singlet channel is

$$\phi_{SO} = eV(t_1 - t_2)/(2\hbar) + \sigma\mu_B B(t_1 + t_2)/\hbar.$$

Hence, the voltage-dependent contribution to the phase is not proportional to the field-dependent contribution. The ratio of these two contributions varies randomly among different pairs of trajectories. So fluctuations in conductance versus field should be uncorrelated with fluctuations in conductance versus voltage. However, Fig. 4 is contrary to what one would expect for strong SO scattering ($\tau_{so} \ll t$). Then it follows that the SO scattering is not strong ($\tau_{so} > t$).

The typical time of flight (t) can be obtained from the correlation energy E_C as $E_C = h/t$. E_C is the interval of electronic energies within which the electronic wavefunctions are correlated in space. It can be measured from the correlation voltage (V_C) as $E_C = V_C/e$, [14] the characteristic voltage scale for the fluctuations in conductance with bias voltage. V_C is roughly equal to the spacing between lines in Fig. 4 along the direction parallel to the bias-voltage axes.

The correlation voltage is obtained from the voltage correlation function $Y(V)$, as $Y(V_C) = 0.5Y(0)$, where $Y(V) = \overline{G(V,B')G(0,B')} - \overline{G(V,B')}\,\overline{G(0,B')}$ and averaging is over B'. We obtain $V_C(0) = 31\mu V$ and $104\mu V$ in samples 1 and 2, respectively. It follows that $\tau_{so} > 1.3 \cdot 10^{-10}$s and $\tau_{so} > 4 \cdot 10^{-11}$s in samples 1 and 2, respectively. By comparison, τ_{so} measured in weak-disordered gold films with resistivity $\rho \approx 66\mu\Omega cm$ is $1.9{\cdot}10^{-13}$s, [16] at least three orders of magnitude shorter than τ_{so} in our nanojunctions. This is the main finding of this paper.

The suppression of SO scattering in our samples can be explained by the granular model described in the introduction. We extract α from τ_{so} measured by weak-localization in thin films of Au, [16] $\alpha \approx 5 \cdot 10^{-3}$. In this case we obtain $D^\star \sim \lambda_F/\sqrt{\alpha} \approx 7nm$. The scattering ratio α can also be extracted from energy level spectroscopy of nanometer scale Au grains. [17] In this case, we find that α varies among different grains, $0.01 < \alpha < 0.05$. Thus 2.2nm$< \lambda_F/\sqrt{\alpha} <$ 5nm.

For example, assume $D = 3nm$ and $\alpha = 0.01$. From resistivity we obtain $R_g \approx \rho/D = 4 \cdot 10^5\Omega$, and Eq. 1 predicts $\tau_{so} \approx 2.3 \cdot 10^{-10}$s.

In conclusion, we have demonstrated that the magnetofingerprints in strong-disordered Au nanojunctions are spin-based. The signature of spin-based magnetofingerprints is a structure in conductance that shifts linearly with bias voltage and magnetic field. The linear structure requires that the transport time (or the dephasing time) be shorter than or comparable to the SO scattering time, which we use to estimate a lower bound of the SO scattering time. The SO scattering time in strong-disordered samples is enhanced by at least three orders of magnitude relative to that in weak-disordered thin films. Granularity and frozen spin-orbit scattering inside the grains suppresses spin-orbit scattering. We propose a generalization of the Elliot-Yafet relation that applies to strong-disordered granular samples and that agrees with our observations.

As a final note, electron spins confined in quantum dots have been proposed as candidate quantum bits, because spin is stable for zero-dimensional systems. [18] In this paper, we show that, without quantum dots, a distributed strong-disordered system has a similar spin stability. This may be an alternate route for the fabrication of solid-state devices with high spin-stability.

We thank A. L. Korotkov for useful discussions. This work was performed in part at the Cornell Nanofabrication Facility, (a member of the National Nanofabrication Users Network), which is supported by the NSF, under grant ECS-9731293, Cornell University and Industrial affiliates, and the Georgia-Tech electron microscopy facility. This research is supported by the David and Lucile Packard Foundation grant 2000-13874 and the NSF grant DMR-0102960.

[1] S. A. Wolf, D. D. Awschalom, R. A. Buhrman, J. M. Daughton, S. von Molnar, M. L. Roukes, A. Y. Chtchelkanova, and D. M. Treger, Science **294**, 1488 (2001).
[2] R. J. Elliot, Phys. Rev. **96**, 266 (1954).
[3] Y. Yafet, Sol. State Phys. **14**, 1 (1963).
[4] F. J. Jedema, M. S. Nijboer, A. T. Filip, and B. J. van Wees, Phys. Rev. B **67**, 085319 (2003).
[5] I. S. Beloborodov, K. B. Efetov, A. V. Lopatin, and V. M. Vinokur, Phys. Rev. Lett. **91** (2003).
[6] P. W. Brouwer, X. Waintal, and B. I. Halperin, Phys. Rev. Lett. **85**, 369 (2000).
[7] K. A. Matveev, L. I. Glazman, and A. I. Larkin, Phys. Rev. Lett. **85**, 2789 (2000).
[8] A. Anaya, A. L. Korotkov, M. Bowman, J. Waddell, and D. Davidović, Journal of Applied Physics **93**, 3501 (2003).
[9] M. Bowman, A. Anaya, A. L. Korotkov, and D. Davidović, Phys. Rev. B **69**, 205406 (2004).
[10] F. J. R. Nieto, G. Andreasen, M. E. Martins, F. Castez, R. C. Salvarezza, and A. J. Arvia, J. Phys. Chem. B **107**, 11452 (2003).
[11] J. E. Grose, A. N. Pasupathy, D. C. Ralph, B. Ulgut, and H. D. Abruna, Phys. Rev. B. **71**, 035306 (2005).
[12] V. Chandrasekhar, Z. Ovadyahu, and R. A. Webb, Phys. Rev. Lett **67**, 2862 (1991).
[13] Y. Imry, *Introduction to mesoscopic physics* (Oxford University Press, 1997).
[14] S. Washburn and R. A. Webb, Rep. Prog. Phys. **55**, 1311 (1992).
[15] B. L. Altshuler and A. G. Aronov, in *Electron-Electron Interactions in Disordered Systems*, edited by A. L. Efros and M. Pollak (Elsevier and Amsterdam, 1985).
[16] G. Bergman, Z. Phys. B **48**, 5 (1982).
[17] J. R. Petta and D. C. Ralph, Phys. Rev. Lett **87**, 266801 (2001).
[18] A. V. Khaetskii and Y. V. Nazarov, Phys. Rev. B **61**, 12639 (2000).